Materials Science & Engineering A 682 (2017) 323–331

Contents lists available at ScienceDirect

Materials Science & Engineering A

journal homepage: www.elsevier.com/locate/msea

High temperature thermal stability of nanocrystalline 316L stainless steel processed by high-pressure torsion

Moustafa El-Tahawy[a,b], Yi Huang[c], Hyelim Choi[d], Heeman Choe[d], János L. Lábár[a,e], Terence G. Langdon[c], Jenő Gubicza[a,*]

[a] Department of Materials Physics, Eötvös Loránd University, P.O.B. 32, Budapest H-1518, Hungary
[b] Department of Physics, Faculty of Science, Tanta University, 31527 Tanta, Egypt
[c] Materials Research Group, Faculty of Engineering and the Environment, University of Southampton, Southampton SO17 1BJ, UK
[d] School of Advanced Materials Engineering, Kookmin University, 77 Jeongneung-ro, Seongbuk-gu, Seoul 136-702, Republic of Korea
[e] Institute for Technical Physics and Materials Science, Centre for Energy Research, Hungarian Academy of Sciences, Budapest, Hungary

ARTICLE INFO

Keywords:
Activation energy
Differential scanning calorimetry
High-pressure torsion
Phase transformation
Stainless steel

ABSTRACT

Differential scanning calorimetry (DSC) was used to study the thermal stability of the microstructure and the phase composition in nanocrystalline 316L stainless steel processed by high-pressure torsion (HPT) for ¼ and 10 turns. The DSC thermograms showed two characteristic peaks which were investigated by examining the dislocation densities, grain sizes and phase compositions after annealing at different temperatures. The first DSC peak was exothermic and was related to recovery of the dislocation structure without changing the phase composition and grain size. The activation energies for recovery after processing by ¼ and 10 turns were ~163 and ~106 kJ/mol., respectively, suggesting control by diffusion along grain boundaries and dislocations. The second DSC peak was endothermic and was caused by a reverse transformation of α'-martensite to γ-austenite. The hardness of annealed samples was determined primarily by the grain size and followed the Hall–Petch relationship. Nanocrystalline 316L steel processed by HPT exhibited good thermal stability with a grain size of ~200 nm after annealing at 1000 K and a very high hardness of ~4900 MPa.

1. Introduction

Austenitic 316L stainless steel is widely used as a structural material in medical applications such as orthopaedic implants [1,2]. In addition, it is used also as a standard construction material in engineering applications and nuclear power facilities due to its superior mechanical properties such as high strength, good ductility, high fracture toughness, excellent corrosion resistance and a low rate of absorption for neutron radiation [3,4]. In practice, 316L stainless steel has been studied extensively in order to further improve the thermal and mechanical properties through tailoring of its microstructure and chemical composition [4-7].

Severe plastic deformation (SPD) is often used for refining the microstructure of bulk solids and generally it also yields an improvement in the mechanical properties [8-10]. High-pressure torsion (HPT) is one of the most effective SPD methods for processing ultrafine-grained (UFG) or nanocrystalline microstructures [11] and results have shown that the grain size of 316L can be refined to the nanocrystalline range by HPT processing [5,12,13]. In addition to grain refinement, a simultaneous phase transformation also occurs during HPT with the transformation sequence γ-austenite → ε-martensite → α'-martensite. It was also revealed that the nanocrystalline grains yielded an exceptionally high hardness of ~6000 MPa after 10 turns of HPT [5]. It should be noted that the ultrahigh-strength martensitic steels often suffer from severe intergranular embrittlement which may lead to shorter operational lifetimes. It is recognized that heat treatment is an effective process to overcome this embrittlement and improve the ductility of martensitic steels [14–17] and it was shown that a heat treatment after deformation of 304L stainless steel led to a reverse martensitic transformation from body-centered cubic (bcc) α'-martensite to face-centered cubic (fcc) γ-austenite [15] thereby yielding a good ductility.

The mechanisms of reverse martensitic transformation and the microstructures of reversed γ-austenite have been investigated in steels with different compositions [18–22]. During annealing, the reversion of α'-martensite to γ-austenite in martensitic steels can occur by two competing mechanisms: the diffusion controlled and the diffusionless shear processes. The prevailing mechanism of α'-martensite reversion is sensitive to the chemical composition of the steel and also to the heat treatment conditions through the temperature [18,20,23–25]. For

* Corresponding author.
E-mail address: jeno.gubicza@ttk.elte.hu (J. Gubicza).

http://dx.doi.org/10.1016/j.msea.2016.11.066
Received 19 October 2016; Accepted 18 November 2016
Available online 19 November 2016
0921-5093/

example, an investigation of the reversion mechanism of α'-martensite to γ-austenite during annealing of rolled stainless steels with two different alloying compositions, namely 16% Cr – 10% Ni and 18% Cr – 9% Ni, showed that the 50% α'-martensite reversion temperature is about 823 K in both steels despite the different mechanism of reversion [24]. For these two compositions the reverse transformation occurred by diffusionless and diffusional processes, respectively. In addition to the chemical composition, the temperature of annealing and the degree of pre-deformation also influence the mechanism of reverese martensitic transformation [18–20,23]. The diffusional reversion is facilitated by the application of plastic deformation prior to annealing and this mechanism normally takes place over a wide temperature range [19]. By contrast, diffusionless shear reversion occurs in a narrow temperature range of about 50–75 K and it is essentially independent of the applied pre-deformation.

In an earlier study [5], the evolutions of the dislocation density, grain size and hardness were investigated with increasing numbers of HPT turns at the periphery of 316L steel disks with the number of turns varying between ¼ and 10. It was found that a nanocrystalline microstructure with a very high dislocation density was formed by HPT and simultaneously the initial γ-austenite phase was partly transformed into ε- and α'-martensites. This very fine multiphase microstructure yielded an outstanding hardness (~6000 MPa). The thermal stability of UFG and nanocrystalline microstructures in martensitic steels is an important factor in their structural applications. Therefore, the present study was initiated to examine the stability of the dislocation density, grain size and phase composition in 316L stainless steel samples processed by HPT. The experiments were performed on two samples processed by the lowest (¼) and highest (10) numbers of turns. The temperature ranges and the activation energies of the processes occurring during annealing were determined by differential scanning calorimetry (DSC). This appears to be the first study documenting the concomitant recovery of the dislocation structure and the reverse martensitic transformation during annealing of HPT-processed 316L steel.

2. Experimental material and procedures

The chemical composition of the 316L stainless steel used in this investigation was determined by energy-dispersion X-ray spectroscopy and is shown in Table 1. The initial material was annealed at 1373 K for 1 h and then quenched to room temperature in water to form a coarse-grained single phase γ-austenite. Disks with diameters of ~9.85 mm and thicknesses of ~0.85 mm were prepared and processed by HPT operating under quasi-constrained conditions [26,27], with an applied pressure of 6.0 GPa at room temperature (RT). The HPT deformation was carried out for low (N =¼) and high (N =10) numbers of revolutions. In an earlier study, the microtructures, the phase compositions and the hardness of these HPT-processed UFG 316L samples were studied in detail [5].

DSC was used to investigate the thermal stability of the phase composition and the microstructure at the periphery of the HPT-processed specimens. For DSC, small samples were cut from the peripheral regions of the HPT disks and the DSC was performed in a Perkin Elmer (DSC2) calorimeter at a heating rate of 20 K/min under an Ar atmosphere. In order to determine the activation energies of the processes related to the DSC peaks, the thermograms were measured at different heating rates of 10, 20, 40 and 60 K/min. The maximum temperature of the DSC scans was 1000 K.

Table 1
The concentrations of the main alloying elements for 316L stainless steel used in this study as determined by energy-dispersive X-ray spectroscopy.

Element	Fe	Cr	Ni	Mo	Mn	Si	Cu	Co
wt%	Bal.	17.20	8.97	2.13	1.03	0.77	0.48	≤ 0.35

In order to study the microstructural evolution during annealing, samples were heated to the characteristic temperatures of the thermograms and then quenched to RT. These specimens were mechanically polished using a 2500 grit silicon carbide paper and then the surfaces were electro-polished using an electrolyte with a composition of 70% ethanol, 20% glycerine and 10% perchloric acid (in vol%) in order to remove the uppermost surface layer distorted due to mechanical polishing. The phase composition of the annealed samples was investigated by X-ray diffraction (XRD) that was performed using a high-resolution diffractometer with $CoK_{\alpha 1}$ radiation (wavelength: λ=0.1789 nm). The crystallite size ($<x>_{area}$) and the dislocation density (ρ) in the main phase were evaluated by X-ray line profile analysis (XLPA) using the Convolutional Multiple Whole Profile (CMWP) fitting method [28]. In this method, the diffraction pattern is fitted by the sum of a background spline and the diffraction profiles obtained as the convolution of the instrumental and microstructural peaks. The latter profiles are caused by the finite crystallite size and the dislocations.

To complement the XLPA investigations, the microstructures of the annealed samples were also studied by direct imaging methods. For high temperature annealing, the grain size was sufficiently large to investigate by scanning electron microscopy (SEM) using an FEI Quanta 3D microscope. Electron backscatter diffraction (EBSD) images were taken with a step size of 30 nm and evaluated using OIM software (TexSem Laboratories). The grain size was determined by the OIM program considering only those boundaries having misorientations higher than 15°. At relatively low annealing temperatures, the grain size in the HPT-processed samples remained very small and therefore it was not possible to investigate these microstructures by EBSD. Accordingly, transmission electron microscopy (TEM) was performed for a determination of the grain size in these specimens. The TEM used a Philips CM20 electron microscope operating at 200 keV, the TEM images were recorded on imaging plates and the diffraction patterns were indexed using the ProcessDiffraction program [29,30].

The stability of the microstructure was also monitored by measuring the Vickers microhardness as a function of the annealing temperature using a Zwick Roell ZHμ hardness tester with an applied load of 500 g and a dwell time of 10 s.

3. Experimental results

3.1. Microstructures and phase compositions in the initial and the HPT- processed specimens

The microstructure and the phase composition of the initial undeformed material and the samples processed by N =¼ and 10 turns of HPT were reported in detail earlier [5]. Specifically, the initial material was almost single phase γ-austenite with an average grain size of ~42 μm and a hardness of ~1400 MPa. During HPT deformation, the γ-austenite was transformed gradually to ε- and α'-martensites. After ¼ turn, the grain size was refined to ~120 nm while the dislocation density increased to ~66×10^{14} m^{-2} in the main α'-martensite phase at the periphery of the disk. Both the grain size and the dislocation density saturated at the disk edge after 10 HPT revolutions with values of ~45 nm and ~133×10^{14} m^{-2}, respectively. This very small grain size after 10 turns yielded a four-fold increase in hardness to ~6000 MPa.

3.2. DSC analyses of the samples processed by HPT

Fig. 1 shows the DSC thermograms taken at a heating rate of 20 K/min for the peripheral parts of the disks processed by HPT for N =¼ and 10 turns. For both specimens, an exothermic DSC peak was observed in the temperature range between ~590 and ~740 K. The temperature of the peak maximum was ~690 K and the released heat,

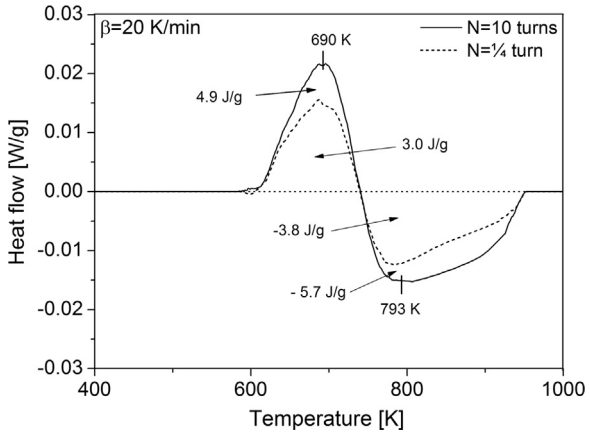

Fig. 1. DSC thermograms obtained at a heating rate of 20 K/min for the peripheral parts of HPT disks processed for N =¼ and 10 turns.

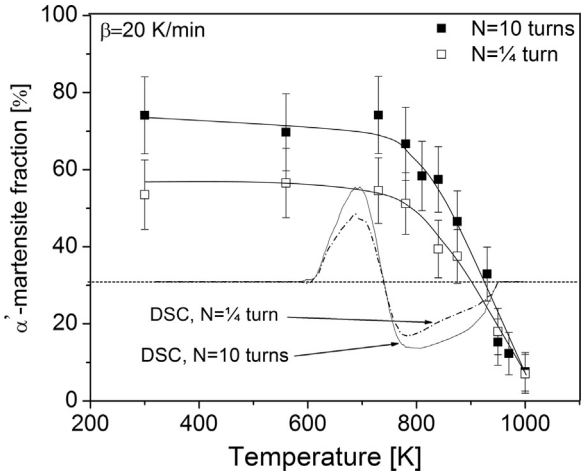

Fig. 3. α'-martensite fraction versus annealing temperature for the HPT samples processed by ¼ and 10 turns. The corresponding DSC thermograms are also shown in the figures.

determined as the areas under the exothermic peaks, had values of ~3.0 and ~4.9 J/g for ¼ and 10 revolutions, respectively. Thus, the released heat was larger after more severe deformation. At about 740 K an endothermic DSC peak started for the two HPT-processed samples and this ended at ~950 K irrespective of the numbers of turns. The peak minimum occurred at ~793 K. The areas under the endothermic peaks for ¼ and 10 revolutions were −3.8 and −5.7 J/g, respectively. The processes related to the exothermic and endothermic peaks were revealed by annealing specimens to different temperatures and studying their phase compositions and microstructures after quenching to RT. These results are now considered.

3.3. Changes of phase composition during DSC annealing

In order to determine the change of phase composition during the DSC heat treatment, XRD measurements were carried out on samples heated to various temperatures. Fig. 2a and b show the X-ray diffractograms obtained for the periphery of the disks processed for N =¼ and 10 turns, respectively, after annealing at different temperatures. The volume fractions of the different phases were estimated from the integrated intensities under the XRD peaks. Due to the small fraction of ε-martensite and the strong overlapping of its XRD peaks with the reflections of γ-austenite, the fraction of ε-martensite was not determined separately but rather this phase was considered as a part of γ-austenite. This evaluation method is in accordance with the concept which considers ε-martensite as a heavily faulted fcc γ-austenite structure with a special arrangement of stacking faults [31]. Fig. 3 shows the fraction of α′-martensite as a function of the annealing temperature at a heating rate of 20 K/min for N =¼ and 10 turns. Immediately after HPT, the values of the α′-martensite fraction were ~53 and ~74% for ¼ and 10 revolutions, respectively. The higher amount of α′-martensite for 10 turns is attributed to the larger strain since the formation of this phase from γ-austenite was induced by the deformation applied during HPT.

For both ¼ and 10 turns, the amounts of α′-martensite practically remained unchanged until the end of the exothermic peak at ~740 K. Above this temperature, the fraction of α′-martensite gradually decreased as this phase was transformed into γ-austenite. Achieving the highest temperature applicable in the present DSC experiments (~1000 K), the fraction of α′-martensite was reduced to about ~7% for both HPT-processed materials where this value is approximately the same as the fraction of α′-martensite observed in the initial material [5]. The remaining α′-martensite in the present HPT-processed materials annealed at 1000 K is in accordance with other reports as a nearly complete reversion of α′-martensite to γ-austenite was only observed beyond 1023 K for a cold-rolled 301LN steel [17].

Comparing the evolution of the fraction of α′-martensite with the DSC thermogram in Fig. 3, it is evident that the endothermic peak is related to the reverse transformation of α′-martensite to γ-austenite. However, it is noted that the endothermic peak apparently finishes before the end of the phase transformation. Indeed, at the end of the endothermic peak at ~950 K there remains about 15% of α′-martensite. This apparent contradiction can be explained by a concomitant

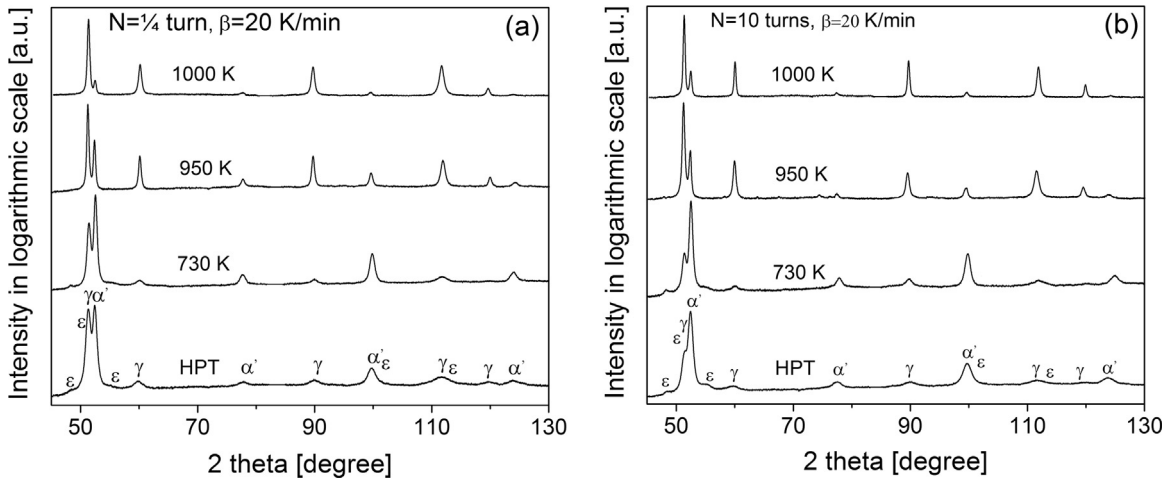

Fig. 2. X-ray diffractograms obtained for the samples processed by HPT and post-annealed at different temperatures. (a) N =¼ turn and (b) N =10 turns.

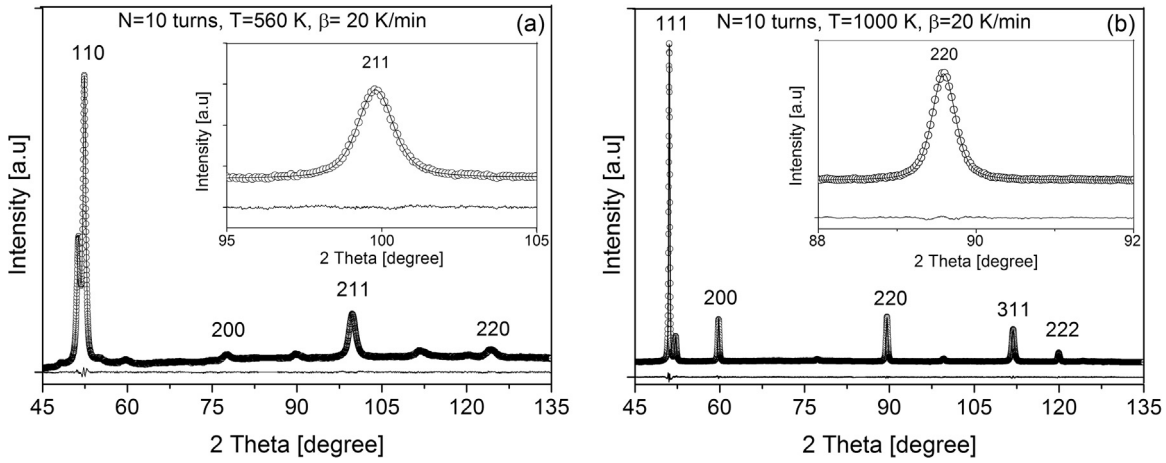

Fig. 4. Fitting on the XRD patterns taken on the samples processed by 10 turns of HPT and heated up to (a) T=560 K and (b) T=1000 K. The open circles and the solid line represent the measured and the fitted patterns, respectively. The difference between the measured and fitted diffractograms is shown at the bottom of the figure. The insets show selected peaks with higher magnification.

exothermic process related to the recovery of the microstructure as described in the following section. Below 950 K, the energy absorbed by the phase transformation overwhelms the heat released due to recovery and at the same time above 950 K the phase transformation slows down resulting in an approximate balance between the absorbed and released heats.

3.4. Microstructure evolution during annealing

The change of the dislocation density and the crystallite size during DSC annealing was studied by XLPA on samples heated to different temperatures. The evaluation of the microstructure was carried out only for the main phase which had the highest fraction among the different crystalline phases. Fig. 3 shows that the α′-martensite remained the major phase for ¼ and 10 turns at annealing temperatures lower than 840 and 875 K, respectively, whereas above these temperatures the γ-austenite became the main phase. Fig. 4a and b illustrate the XLPA fitting for the bcc α′-martensite and the fcc γ-austenite main phases in the samples processed by 10 turns and annealed at 560 and 1000 K, respectively. In Fig. 4a the four peaks of the major α′-martensite phase measured in the Bragg angle range of 45–135° by CoKα$_1$ radiation were fitted by the CMWP method while the other peaks related to the γ-austenite and ε-martensite phases were put into the background. At the same time, in Fig. 4b γ-austenite is the main phase and therefore the fitting was carried out only for the X-ray peaks related to this fcc structure. In both cases, the difference between the measured and the fitted diffractograms was practically zero, thus indicating a good fitting of the measured diffractogram by the theoretical pattern.

Fig. 5 shows the evolution of the dislocation density and crystallite size in the main phase as a function of the annealing temperature for N =¼ and 10 turns. It can be seen that the dislocation density in the main α′-martensite phase practically remains unchanged during annealing up to the beginning of the exothermic DSC peak. For 10 turns of HPT, in the temperature range corresponding to the exothermic DSC peak, the dislocation density decreased from ~133×10^{14} to ~50×10^{14} m^{-2}. Similarly, for N =¼ the dislocation density decreased from ~66×10^{14} to ~39×10^{14} m^{-2} during the exothermic peak. The crystallite size remained practically unchanged during the exothermic DSC peak for ¼ turn and there was only a slight increment for 10 turns.

It should be noted that in severely deformed metallic materials the crystallite size corresponds to the subgrain size rather than to the grain size determined by microscopic methods. Therefore, the grain size was also determined by TEM at the characteristic temperatures of the DSC

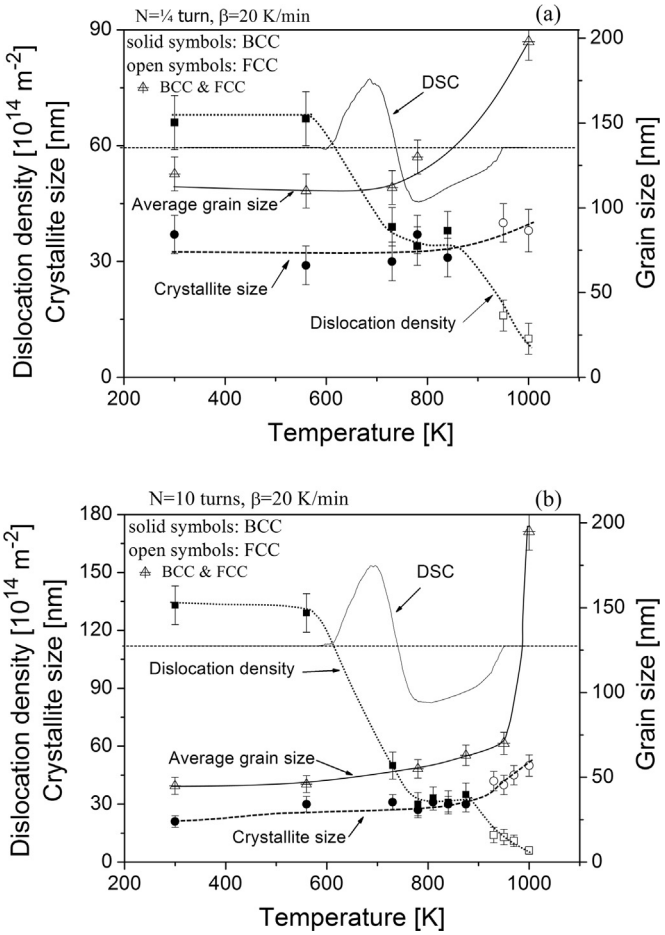

Fig. 5. The average grain size obtained by TEM and EBSD, and the crystallite size and dislocation density determined by XLPA as function of annealing temperature for the main phase in the samples processed by HPT for (a) N =¼ turn and (b) N =10 turns. The corresponding DSC thermograms are also shown in the figures.

thermograms. Fig. 6 shows dark field TEM images for the HPT samples processed by 10 turns and annealed to different temperatures. For each specimen, the average grain size was calculated from an evaluation of about 50–100 grains. Thus, similar to the crystallite size, the grain size also remained unchanged within the experimental error during the exothermic peak as revealed in Fig. 5. Therefore, it can be concluded that in the first and exothermic DSC peak a recovery of the dislocation

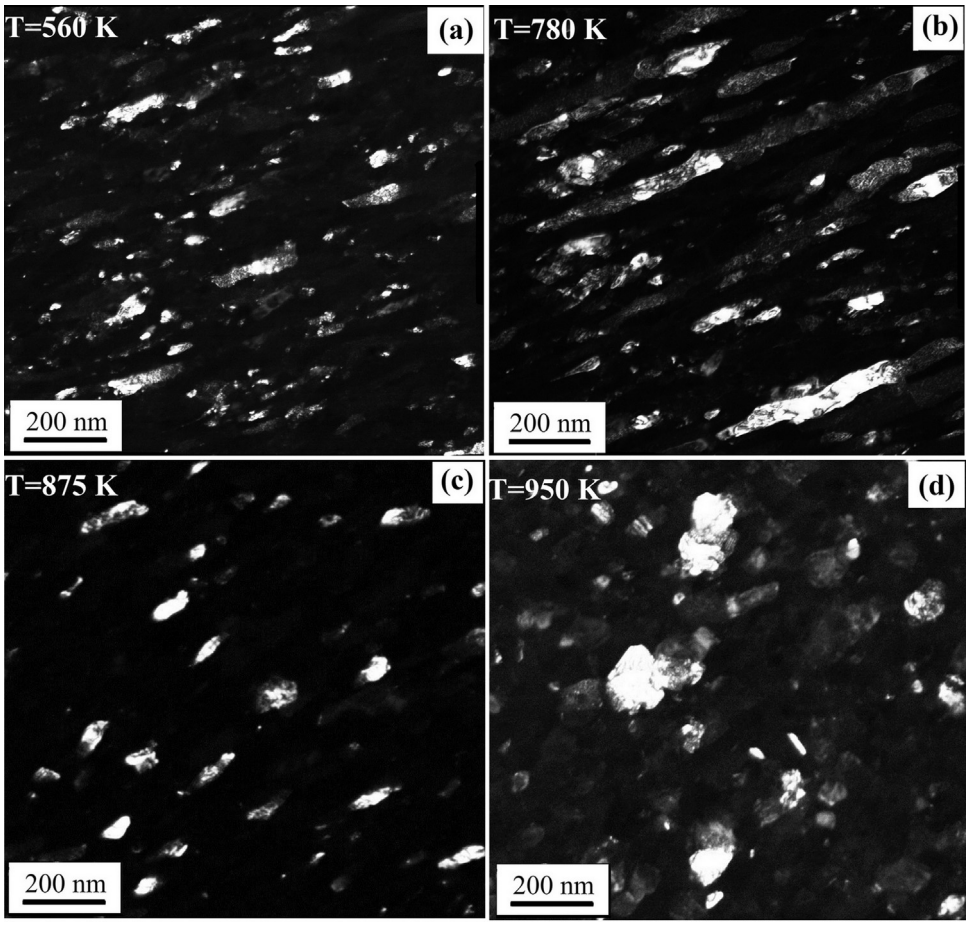

Fig. 6. TEM images obtained for the samples processed for 10 turns and annealed at (a) 560 K, (b) 780 K, (c) 875 K and (d) 950 K.

structure occurred without any significant grain-growth.

In the first and major part of the second and endothermic peak, between 740 and 875 K, both the crystallite size and the dislocation density showed little change in the main α′-martensite phase as demonstrated in Fig. 5. At the same time, the fraction of α′-martensite decreased from ~54 to ~38% and from ~74 to ~47% for ¼ and 10 turns, respectively (see Fig. 3). The unchanged dislocation density is most probably caused by a balance between the annihilation of dislocations due to annealing and their formation owing to the stresses induced by the phase transformation. Earlier studies [32] showed that the phase transformation of α′-martensite to γ-austenite is accompanied by a volume contraction which may yield internal stresses and the formation of lattice defects. Indeed, it was revealed that vacancy clusters consisting of ~6–9 vacancies formed at the interface between α′-martensite and γ-austenite after the reverse phase transformation [32].

In the first part of the endothermic peak, only a moderate increase of the grain size of less than ~30% was observed. In the last and short part of the endothermic peak between 875 and 950 K the phase transformation was accelerated and the fraction of the α′-martensite phase decreased to ~15% as shown in Fig. 3. In this temperature range, the main phase is γ-austenite and the dislocation density decreased rapidly to ~13–14×10^{14} m^{-2} for both ¼ and 10 turns. Above 950 K the reduction of the α′-martensite fraction continued without any endothermic DSC signal. Most probably, the effect of this phase transformation on the thermogram was compensated by an exothermic signal due to the decrease in the dislocation density and the increase of the grain size. Indeed, Fig. 5 shows that in the temperature range of 950–1000 K the dislocation density decreased from ~13–14×10^{14} m^{-2} to ~6–10×10^{14} m^{-2} while the grain size increased very rapidly to ~195–198 nm for the two samples processed by ¼ and 10 revolutions. The final microstructures after heating the samples processed by ¼ and 10 turns to 1000 K are shown in the EBSD images of Fig. 7. In accordance with the XRD results, these EBSD images reveal that the reverse transformation of α′-martensite to γ-austenite is incomplete even at 1000 K and about 7% of α′-martensite remains in the microstructure.

It is important to note that the HPT-processed 316L steel samples exhibited very good thermal stability since, even after annealing up to 1000 K, the dislocation density remained high at ~6–10×10^{14} m^{-2} while the average grain size remained not higher than ~200 nm. Indeed, the continuous Debye-Scherrer XRD rings observed in the imaging plates for both samples annealed up to 1000 K suggest that no recrystallization occurred over this temperature range. This observation is consistent with previous studies which showed that recrystallization in cold rolled 316L steel occurred only above ~1025 K [24]. It was also shown that in nanocrystalline 316L steel doped with Al there was a significant grain growth only after completion of the reverse phase transformation to γ-austenite [25]. The very good thermal stability of the UFG and nanocrystalline microstructures in γ-austenite is due to the high melting point of ~1700 K [33] and the high concentration of alloying elements. Both of these characteristics hinder the climb and cross-slip of dislocations which are fundamental recovery processes.

3.5. Influence of the DSC heat treatment on hardness

Fig. 8 shows the Vickers microhardness as a function of the annealing temperature for N =¼ and 10 turns. It is evident that the hardness remained practically unchanged up to ~900 K for both

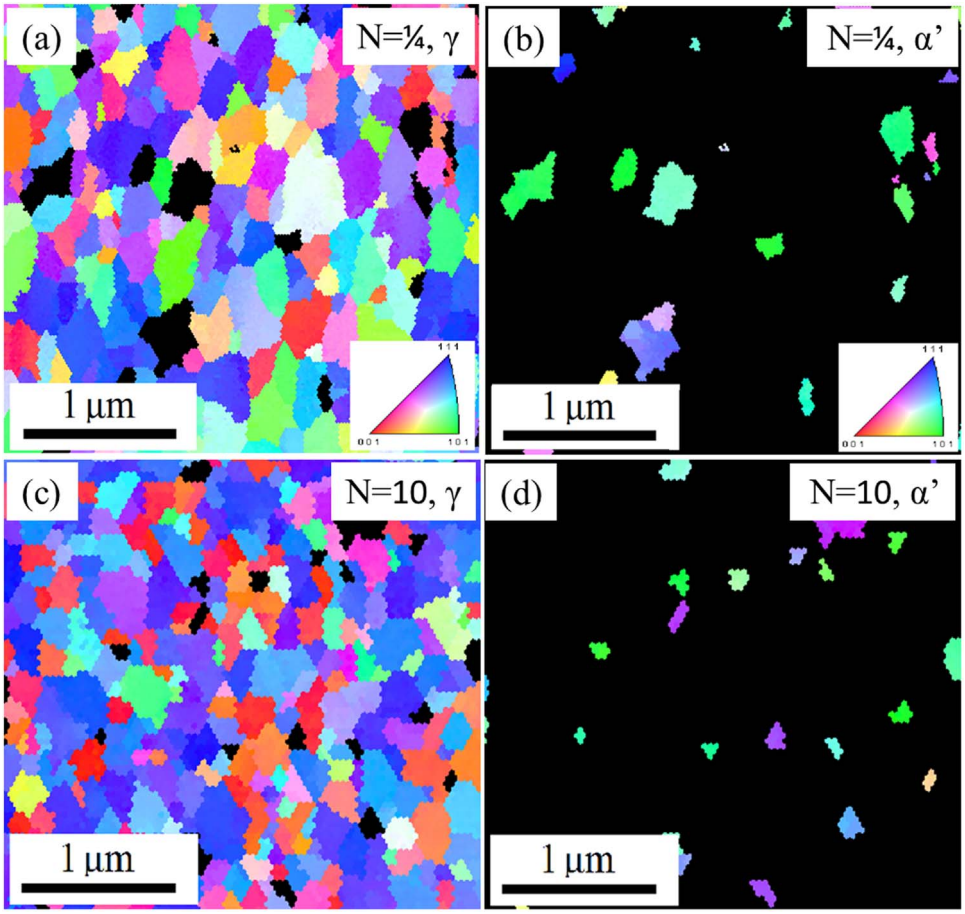

Fig. 7. EBSD images showing the grain structure after annealing at 1000 K for (a) γ-austenite and (b) α'-martensite in the sample processed for ¼ turn, and for (c) γ-austenite and (d) α'-martensite in the specimen processed for 10 turns.

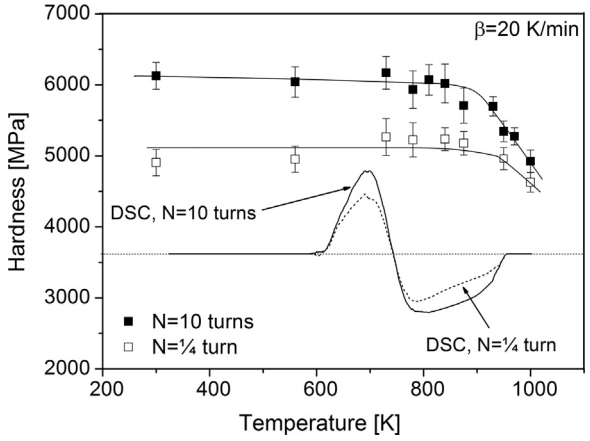

Fig. 8. The hardness versus the annealing temperature for N =¼ and 10 turns. The corresponding DSC thermograms are also shown in the figures.

materials. This temperature corresponds to the end part of the endothermic peak and therefore it is concluded that neither the recovery of the dislocation structure nor the extensive phase transformation influences the hardness of the nanostructured 316L steel processed by HPT. At the same time, when the grain size started to grow at the end of the endothermic peak, the hardness was reduced especially for the material processed by 10 turns (compare for example, Figs. 5 and 8). This observation suggests that the hardness is influenced mainly by the grain size. The higher decrease of the hardness for 10 turns is due to the larger degree of grain growth from ~45 to ~195 nm compared to the grain coarsening for ¼ turn from ~120 to ~198 nm.

This result is in agreement with the previous study which showed that the hardness of 316L steel samples processed by HPT were more sensitive to the grain size than the phase composition [5]. Other investigations also found that the recovery makes only a small contribution to softening in steels having low stacking fault energies [34]. It is worth noting that the hardness remained high at ~4900 MPa even after annealing up to 1000 K for both N =¼ and 10 turns. As the initial material was also a nearly single phase γ-austenite, the combination of HPT and annealing up to 1000 K enhanced the mechanical strength of 316L stainless steel without introducing any significant change in the phase composition.

3.6. Activation energies determined from the DSC thermograms

This study revealed that the first, exothermic peak in the DSC thermograms is related to the recovery of the microstructure in nanocrystalline 316L steel processed by HPT. The activation energy of the recovery was estimated from the shift of the exothermic peak maximum when the heating rate was varied. The analysis was carried out using the Kissinger equation [35]:

$$ln\frac{\beta}{T_P^2}=-\frac{Q}{k}\frac{1}{T_P}+B, \quad (1)$$

where β is the heating rate, T_P is the temperature of the peak maximum, Q is the activation energy, k is the Boltzmann constant and B is a constant. The values of Q and B can be determined from the slope and the intercept of the straight line fitted to datum points in the plot $ln\frac{\beta}{T_P^2}$ versus $\frac{1}{T_P}$.

Fig. 9 shows the Kissinger plots for the samples processed by HPT

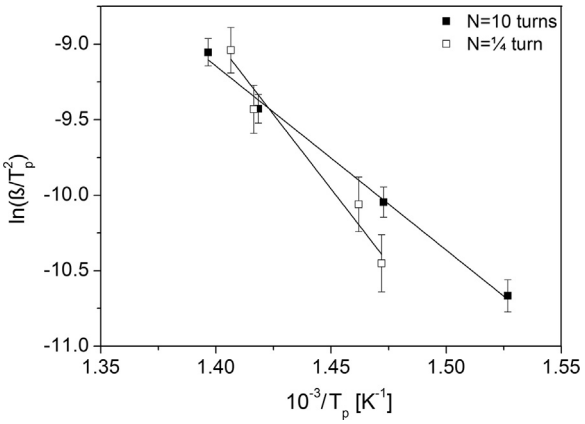

Fig. 9. Kissinger plot for the evaluation of the activation energy of recovery from $ln(\beta/T_P^2)$ versus $1/T_P$. β is the heating rate and T_P is the temperature of DSC peak maximum.

for N =¼ and 10 turns. The values of the activation energies for recovery are ~163 ± 19 and ~106 ± 10 kJ/mol for ¼ and 10 turns, respectively. In the temperature range related to the endothermic peak, in addition to the reverse transformation from α′-martensite to γ-austenite, a recovery of the dislocation structure and grain growth also occurred. Therefore, the activation energy of the reverse martensitic phase transformation cannot be determined from the shift of the endothermic peak due to the variation in the DSC heating rate.

4. Discussion

4.1. Correlation between the microstructure and the activation energy of recovery

The activation energies for self-diffusion in pure iron with fcc and bcc structures are ~278 kJ/mol [36] and ~255 kJ/mol [37,38], respectively, and the activation energies for diffusion along grain boundaries and dislocations are about one-half of the value for self-diffusion in coarse-grained materials [39,40]. Thus, the activation energy for grain boundary and bulk diffusion of iron in Fe–20Cr–25Ni–Nb stainless steel is ~178 and ~278 kJ/mol, respectively [41] and the activation energy for grain boundary diffusion of iron in 316 stainless steels is ~173 kJ/mol [42]. These values are close to the activation energies of recovery determined in the present study.

Thus, the DSC investigations showed that the activation energies of recovery for nanocrystalline 316L steel processed by ¼ and 10 HPT turns are smaller than the activation energy of self-diffusion in iron by factors of about 0.6 and 0.4, respectively. This suggests that recovery is controlled by diffusion along the grain boundaries and dislocations. Indeed, the grain size remained as small as ~50–110 nm and the dislocation density was reduced to ~40–50×10^{14} m^{-2} during the exothermic DSC peak for both ¼ and 10 turns so that relatively fast diffusion along the lattice defects determined the rate of recovery. It is noted, however, that a significantly higher activation energy for recovery was observed for the sample processed through ¼ turn compared to 10 turns. This difference is attributed to the lower frequency of diffusion short circuits in the sample processed by ¼ turn due to the inherently larger grain size and the smaller dislocation density. In addition, the higher fraction of γ-austenite after ¼ turn may also contribute to the higher activation energy of recovery since diffusion in the fcc iron structure is more difficult than in the bcc phase as shown by the higher self-diffusion activation energy [36–38].

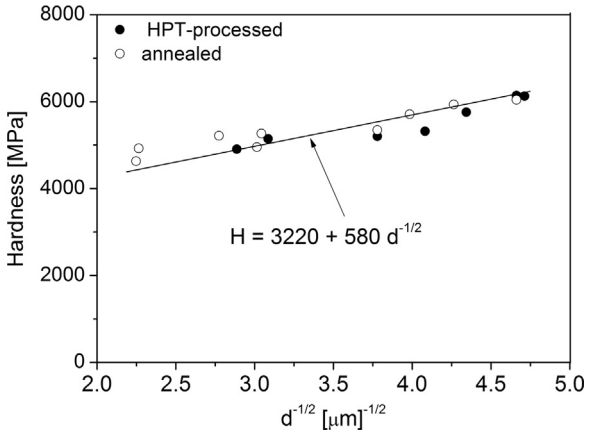

Fig. 10. Hall–Petch plot of the relationship between the hardness (H) and the grain size (d) measured on HPT processed 316L steel samples (the data were taken from [5] and represented by solid circles) and after annealing the specimens processed for ¼ and 10 turns of HPT (the data are from this study and denoted by open circles).

4.2. Hall–Petch relationship between the hardness and the grain size during annealing

In an earlier study [5], it was shown that the hardness of HPT-processed 316L samples was determined primarily by the grain size. Even if the phase compositions were very different, samples with similar grain sizes exhibited similar hardnesses while the various different grain sizes yielded very different hardness values. It was also shown that the hardness (H) versus grain size (d) data for 316L steel obeyed the Hall-Petch relationship [43,44]:

$$H=H_0+k_H d^{-0.5}. \quad (2)$$

In practice, the values of H_O and k_H depend on the precise grain size regime. For grain sizes larger than 1 μm H_O ≈745 MPa and k_H ≈2804 MPa $\mu m^{1/2}$, while for UFG materials the values of H_O and k_H were ~3220 MPa and ~580 MPa $\mu m^{1/2}$, respectively [5]. Comparing the microstructural parameters, the phase fractions and the hardness values obtained for different annealing temperatures in Figs. 3, 5 and 9, it appears that the hardness is primarily determined by the grain size also for the annealed nanocrystalline 316L steel samples. In Fig. 10 the hardness values are plotted as a function of $d^{-1/2}$ for 316L steel samples immediately after HPT processing (denoted by solid symbols) and after post-annealing in DSC up to different temperatures (denoted by open symbols). The data for the HPT samples were measured at the peripheries of disks processed for different numbers of turns [5]. In Fig. 10 the nine datum points for the post-annealed samples represent the states for which the grain size values were determined (see Fig. 5). The straight line in the Hall–Petch plot was obtained by fitting the data obtained for the HPT-processed samples in the earlier study [5]. It can be seen that the data obtained on the annealed HPT samples (indicated by open circles) follow the same Hall–Petch relationship despite the strong reduction in the dislocation density and the change in the phase composition. Therefore, it is concluded that neither the occurrence of recovery nor the reverse phase transformation from α′-martensite to γ-austenite influences the hardness evolution during the annealing of nanocrystalline 316L steel.

5. Summary and conclusions

1. The thermal stability of the nanocrystalline microstructure in 316L stainless steel processed by HPT for ¼ and 10 turns was investigated by DSC up to 1000 K. Two peaks were observed in the DSC thermograms for both materials. The first, an exothermic peak, was detected between ~590 and ~740 K and related to the annihilation of dislocations. During this recovery, the phase composition and the

average grain size remained practically unchanged. The second, an endothermic peak between ~740 and ~950 K, was caused by a reverse phase transformation of α'-martensite to γ-austenite and the reverse phase transformation continued even after the end of the endothermic peak. Between ~950 and ~1000 K the heat absorbed by the phase transformation was compensated by the heat released due to recovery and grain growth.

2. There was no influence of the number of HPT turns on the temperature range of the DSC peaks despite the different grain sizes, phase compositions and dislocation densities in samples processed for ¼ and 10 turns. The activation energies of recovery were different at ~163 and ~106 kJ/mol for ¼ and 10 turns, respectively, and these values suggest that recovery is controlled by diffusion along the grain boundaries and dislocations.
3. The HPT-processed nanocrystalline 316L steel samples exhibited very good thermal stability such that, even after heat treatments performed up to 1000 K, high dislocation densities of ~6–10×10^{14} m^{-2} and small grain sizes of ~200 nm remained in the materials. This good stability is attributed to the large alloying element concentration and the high melting point of 316L steel.
4. Despite the significant decrease in the dislocation density and the extensive phase transformation, the hardness changed only slightly up to the end of the endothermic peak. Above ~950 K the hardness decreased rapidly due to grain growth. Therefore, the hardness of annealed nanocrystalline 316L steel is determined primarily by the grain size and the hardness values follow the Hall–Petch relationship
5. The initial 316L steel material before HPT was an almost single phase γ-austenite with an average grain size of ~42 μm. HPT processing gave a partial phase transformation to α'-martensite and simultaneous grain refinement while annealing up to 1000 K yielded an almost complete reverse transformation to γ-austenite without any major grain growth. The relatively small grain size yielded a high hardness with a value of ~4900 MPa. It is concluded that a combination of HPT at RT and annealing up to 1000 K is a powerful method for achieving a fully austenitic UFG microstructure with a high strength in 316L stainless steel.

Acknowledgements

This work was supported by the Hungarian Scientific Research Fund, OTKA, Grant no. K-109021 and the authors are grateful to Mr. Alajos Ö. Kovács and Mr. Gábor Varga for DSC and EBSD investigations, respectively. The work of two of us was supported by the European Research Council under ERC Grant Agreement No. 267464-SPDMETALS (YH and TGL). Choi and Choe also acknowledge support from the NRF (2015R1D1A1A01060773; 2014R1A2A1A11052513) of Korea.

References

[1] G.L.Lucas, F.W.Cooke, E.A.Friis, Springer Science + Business Media, New York, 1999.
[2] I. Gotman, Characteristics of metals used in implants endourology, Endourology 11 (1997) 383–389.
[3] W. Kim, S. Yoon, W. Ryu, C. Lee, Application of minimum commitment method for predicting long-term creep life of type 316LN stainless steel, J. Korean Inst. Met. Mater. 46 (2008) 118–124.
[4] Y. Kim, Y. Kim, D. Kim, S. Kim, W. Nam, H. Choe, Effects of hydrogen diffusion on the mechanical properties of austenite 316L steel at ambient temperature, Mater. Trans. 52 (2011) 507–513.
[5] J. Gubicza, M. El-Tahawy, Y. Huang, H. Choi, H. Choe, J.L. Lábár, T.G. Langdon, Microstructure, phase composition and hardness evolution in 316L stainless steel processed by high-pressure torsion, Mater. Sci. Eng.: A 657 (2016) 215–223.
[6] N. Tosangthum, O. Coovattanachai, R. Krataitong, M. Morakotjinda, A. Daraphan, B. Vetayanugul, R. Tongsri, Density and strength improvement of sintered 316L stainless steel, Chiang Mai J. Sci. 33 (2006) 53–66.
[7] X.H. Chen, J. Lu, L. Lu, K. Lu, Tensile properties of a nanocrystalline 316L austenitic stainless steel, Scr. Mater. 52 (2005) 1039–1044.
[8] R.Z. Valiev, Y. Estrin, Z. Horita, T.G. Langdon, M.J. Zehetbauer, Y.T. Zhu, Producing bulk ultrafine-grained materials by severe plastic deformation, JOM 58 (4) (2006) 33–39.
[9] R.Z. Valiev, A.P. Zhilyaev, T.G. Langdon, Bulk Nanostructured Materials: Fundamentals and Applications, John Wiley & Sons, Inc, Hoboken, NJ, 2014.
[10] T.G. Langdon, Twenty-five years of ultrafine-grained materials: achieving exceptional properties through grain refinement, Acta Mater. 61 (2013) 7035–7059.
[11] A.P. Zhilyaev, T.G. Langdon, Using high-pressure torsion for metal processing: fundamentals and applications, Prog. Mater. Sci. 53 (2008) 893–979.
[12] Y. Mine, Z. Horita, Y. Murakami, Effect of hydrogen on martensite formation in austenitic stainless steels in high-pressure torsion, Acta Mater. 57 (2009) 2993–3002.
[13] S. Scheriau, Z. Zhang, S. Kleber, R. Pippan, Deformation mechanisms of a modified 316L austenitic steel subjected to high pressure torsion, Mater. Sci. Eng.: A 528 (2011) 2776–2786.
[14] N.H. Heo, Ductile-brittle-ductile transition and grain boundary segregation of Mn and Ni in an Fe-6Mn-12Ni alloy, Scr. Mater. 34 (1996) 1517–1522.
[15] F. Forouzan, A. Najafizadeh, A. Kermanpur, A. Hedayati, R. Surkialiabad, Production of nano/submicron grained AISI 304 L stainless steel through the martensite reversion process, Mater. Sci. Eng.: A 527 (2010) 7334–7339.
[16] T. Roland, D. Retraint, K. Lu, J. Lu, Enhanced mechanical behavior of a nanocrystallised stainless steel and its thermal stability, Mater. Sci. Eng.: A 445–446 (2007) 281–288.
[17] M.C. Somani, P. Juntunen, L.P. Karjalainen, R.D.K. Misra, A. Kyröläinen, Enhanced mechanical properties through reversion in metastable austenitic stainless steels, Metall. Mater. Trans. A 40 (2009) 729–744.
[18] K.B. Guy, E.P. Butler, D.R.F. West, Reversion of bcc: α' martensite in Fe-Cr-N i austen'itic stainless steels, Met. Sci. 17 (1983) 167–176.
[19] S. Takaki, K. Tomimura, S. Ueda, Effect of pre-cold-working on diftusional reversion of deformation induced martensite in metastable austenitic stainless steel, ISIJ Int. 34 (1994) 522–527.
[20] K. Tomimura, S. Takaki, Y. Tokunaga, Reversion mechanism from deformation induced martensite to austenite in metastable austenitic stainless steels, ISIJ Int. 31 (1991) 1431–1437.
[21] R.D.K. Misra, S. Nayak, P.K.C. Venkatasurya, V. Ramuni, M.C. Somani, L.P. Karjalainen, Nanograined/ultrafine-grained structure and tensile deformation behavior of shear phase reversion-induced 301 austenitic stainless steel, Metall. Mater. Trans. A 41 (2010) 2162–2174.
[22] K. Tomimura, S. Takaki, Y. Tokunaga, Reversion process of deformatien induced martensite to austenite in metastable austenitic stainless steels, Tetsu-to-Hagane 74 (1988) 1649–1656.
[23] S. Rajasekhara, L.P. Karjalainen, A. Kyröläinen, P.J. Ferreira, Microstructure evolution in nano/submicron grained AISI 301LN stainless steel, Mater. Sci. Eng., Mater. Sci. Eng.: A 527 (2010) 1986–1996.
[24] C. Herrera, R.L. Plaut, A.F. Padilha, Microstructural refinement during annealing of plastically deformed austenitic stainless steels, Mater. Sci. Forum 550 (2007) 423–428.
[25] A. Almathami, G. Goodall, M. Brochu, Crystal structure, transformation and thermal stability of nanostructured 316LSS alloyed with 2 and 6 wt% aluminum, Mater. Sci. Eng.: A 527 (2010) 6020–6027.
[26] R.B. Figueiredo, P.R. Cetlin, T.G. Langdon, Using finite element modeling to examine the flow processes in quasi-constrained high-pressure torsion, Mater. Sci. Eng. A 528 (2011) 8198–8204.
[27] R.B. Figueiredo, P.H.R. Pereira, M.T.P. Aguilar, P.R. Cetlin, T.G. Langdon, Using finite element modeling to examine the temperature distribution in quasi-constrained high-pressure torsion, Acta Mater. 60 (2012) 3190–3198.
[28] G. Ribárik, J. Gubicza, T. Ungár, Correlation between strength and microstructure of ball-milled Al–Mg alloys determined by X-ray diffraction, Mater. Sci. Eng.: A 387–389 (2004) 343–347.
[29] J.L. Lábár, Consistent indexing of a (set of) single crystal SAED pattern(s) with the ProcessDiffraction program, Ultramicroscopy 103 (2005) 237–249.
[30] J.L. Lábár, M. Adamik, B.P. Barna, Z. Czigány, Z. Fogarassy, Z.E. Horváth, O. Geszti, F. Misják, J. Morgiel, G. Radnóczi, G. Sáfrán, L. Székely, T. Szűts, Electron diffraction based analysis of phase fractions and texture in nanocrystalline thin films, part III: application examples, Microscopy and microanalysis: the official journal of Microscopy Society of America, Microbe. Anal. Soc., Microsc. Soc. Can. 18 (2012) 406–420.
[31] K. Guy, E.P. Butler, D.R.F. West, ε and α' martensite formation and reversion in austenitic stainless steels, J. de Phys. 43 (1982) 575–580.
[32] E. Dryzek, M. Sarnek, M. Wróbel, Reverse transformation of deformation-induced martensite in austenitic stainless steel studied by positron annihilation, J. Mater. Sci. 49 (2014) 8449–8458.
[33] L. Sun, K. Muszka, B.P. Wynne, E.J. Palmiere, On the interactions between strain path reversal and dynamic recrystallisation in 316L stainless steel studied by hot torsion, Mater. Sci. Eng.: A 568 (2013) 160–170.
[34] F. Haebner, R. Plaut, A.F. Padilha, Separation of static recrystallization and reverse transformation of deformation-induced martensite in an austenitic stainless steel by calorimetric measurements, ISIJ Int. 43 (2003) 1472–1474.
[35] H.E. Kissinger, Reaction kinetics in differential thermal analysis, Anal. Chem. 29 (1957) 1702–1706.
[36] A.A. Vasilyev, S.F. Sokolov, N.G. Kolbasnikov, D.F. Sokolov, Effect of alloying on the self-diffusion activation energy in γ-iron, Phys. Solid State 53 (2011) 2194–2200.
[37] D.W. James, G.M. Leak, Self-diffusion and diffusion of cobalt in alpha and delta-iron, Philos. Mag. 14 (1966) 701–713.
[38] Y. Iijma, K. Kimurat, K. Hirano, Self-diffusion and isotope effect in α-iron, Acra Meroll 36 (1988) 2811–2820.

[39] J. Lian, R. Valiev, B. Baudelet, On the enhanced grain growth in ultrafine grained metals, Acta Metall. Mater. 43 (1995) 4165–4417.
[40] S.C. Tjong, H. Chen, Nanocrystalline materials and coatings, Mater. Sci. Eng.: R 45 (2004) 1–88.
[41] A.F. Smith, G.B. Gibbs, Volume and grain-boundary diffusion in 20 Cr/25 Ni/Nb stainless steel, Met. Sci. 3 (1969) 93–94.
[42] R.V. Patil, B.D. Sharma, Lattice and grain-boundary diffusion of ^{59}Fe in 316 stainless steel, Met. Sci. 16 (1982) 389–392.
[43] N.J. Petch, The cleavage strength of polycristals, J. Iron Steel Inst. 174 (1953) 25–28.
[44] E.O.Hall, The Deformation and Ageing of Mild Steel, in: Proceedings Phys. Soc. Lond., B64747-753, 1951.